Journal of the Chinese Society of Mechanical Engineers, Vol.47, No.4, pp329~339 (2026)

Estimating Temperature Fields and Pressure-Viscosity Index Using Inverse Approach in Thermal Elastohydrodynamic Lubrication of Point Contacts

Li-Ming Chu*, Chang-Jian, Cai-Wan**, Yuh-Ping Chang***, and Ming-Jer Hsieh****

Keywords： Inverse approach, TEHL, point contact, temperature, pressure-viscosity index

ABSTRACT

This paper proposed a thermal elasto-hydrodynamic lubrication (TEHL) inverse approach to estimate the pressure distribution, the temperature distribution, and the pressure-viscosity index in an TEHL point contact. Once the film shape is measured, the least-squares criterion is used to obtain the smallest error between the measured and estimated film thickness. Furthermore, the pressure and estimated film thickness distributions can be calculated from force balance and elastic deformation theories. The Newton-Raphson method and the Gauss-Seidel iteration are employed to calculate the temperature distribution from energy, surface temperature, and rheology equations by using these smoothing pressure and estimated film thickness distributions. This inverse approach can effectively overcome pressure and temperature rise fluctuations due to oil film measurement error. This present inverse approach can obtain accurate results of pressure and temperature rise distribution from a small number of measured film thickness points, which also saves computing time. For the measurement error in the film thickness, this approach still gives a quite good solution for the pressure distribution, temperature distribution, and the pressure-viscosity index. This present inverse approach can tolerate larger the film thickness measurement error.

Paper Received June, 2025. Revised June, 2025. Accepted July, 2025.

Author for Correspondence: Li-Ming Chu.

* *Professor, Department of Green Energy and Information Technology, National Taitung University, Taitung City 950309, Taiwan, ROC*

** *Department of Mechanical Engineering, National Chin-Yi University of technology, Taichung City 411030, Taiwan, R.O.C.*

*** *Department of Mechanical Engineering, Kun Shan University, Tainan City 710303, Taiwan, R.O.C.*

**** *Department of Power Mechanical Engineering, National Taitung Junior College, Taitung City, 95092, Taiwan, R.O.C.*

INTRODUCTION

With the development of science and technology, mechanical components are increasingly operating under severe conditions such as high speeds, high temperatures, and heavy loads. Therefore, the contact area will generate elastic deformation, the temperature of the lubricant will rise, the viscosity of the lubricant will decrease rapidly, and the load capacity will reduce. It might lead to failure of lubrication film. Therefore, elastic deformation, hydrodynamic lubrication and thermal effect are very important topic. The working conditions of ball bearing, thrust ball bearing, spherical rolling joint, ball screw etc. are belong to the point contact state. They are widely used in industry. The temperature distribution of millimeter-level point contact can't be correctly measured with current technology. So an accurate estimate of temperature distribution in the thermal elastohydrodynamic lubrication (TEHL) of point contact problem is necessary, but it is lacking.

The thermal effect in elastohydrodynamic lubrication (EHL) has long been a significant topic of research in the field of tribology. Numerous studies have focused on measuring temperature rise within TEHL contacts. Safa et al. (1982) used the thin-film manganin pressure transducers to measure pressure. In addition, they utilized a resistance transducer to measure temperature and a capacitive transducer to measure oil film thickness in lubricated contacts, respectively. They presented experimental relationship between oil film thickness, temperature and pressure using mentioned above transducers in actual roller bearing and disc machine. Kannel et al. (1978) developed a special bisignal transducer to measure pressure and temperature simultaneously. This technique can locate the contact zone temperature relative to pressure and evaluate the relationship between heat generation and pressure. Turchina et al. (1974) and Ausherman et al. (1976) employed an improved infrared radiation emitted technique to measure the detailed mapping for averaged through the thickness temperature of a naphthenic mineral oil and the ball surface temperature in an EHD conjunction. Yagi et al. (2005,2006) used a ball-on-disc apparatus to measure the thickness of the oil film by optical interferometry and to capture the temperature of the ball surface, disc surface, and oil film by infrared technique. The transparent disc without any coating and non-transparent disc with a comparatively thick Cr coating were conducted. These experimental data can describe the mechanism of variations in elastohydrodynamic lubricated oil film under high slip ratio conditions. They demonstrated that the shape of the oil film can be varied by viscosity wedge action which related to pressure and temperature. As mentioned above, only the temperature distribution is measured, the pressure distribution is not measured.

During the last decade, the optical interferometry has been found to be the most widely used method for oil film thickness measurement. Many measurement studies of the EHL oil film thickness were presented (Cyriac et al.,2016, Marx et al.,2016, Lu et al.,2018). This method provides very detailed information of the film thickness between contacting bodies. The contact radius is about sub-millimeter (mm) and the contact oil thickness is sub- micrometer (μm). Their contact region depends on the load. The current pressure measurement technology (Safa et al.,1982, Kannel et al.,1978) cannot reach the sub-millimeter (mm) level and cannot measure the detailed pressure distribution, but can measure the average pressure value between contacting bodies. The measurement of pressure distribution between contacting bodies is still scarce in the literature. Recently, the technology of calculating the pressure distribution by measuring the oil film thickness has been proposed and widely used. When the oil film thickness shape is measured from optical interferometry, the pressure distribution can be computed iteratively by using the force balance and the elastic deformation theories. This calculated pressure distribution and the measured oil film thickness shape can be used to evaluate the viscosity using the Reynolds equation, but these algorithms (Paul and Cameron ,1972, Wong et al.,1992, Astrom and Venner,1994) are easy to diverge due to the oil film error causes the larger pressure error. Ostensen et al. (1996) theoretically investigated the possibility of using optical interferometry for determining pressure and apparent viscosity in an EHL point contact. Results showed that the discontinuities in film thickness cause some fluctuations in pressure, they would result in a large error in calculating viscosity. Hence, Lee et al. (2003) developed an inverse approach to overcome this problem in EHL point contacts. In this algorithm, only a few measured film thickness points are sufficient to estimate the pressure distribution without any fluctuation. But the temperature effect is not considered. Chu et al. (2009) developed an inverse approach to calculate temperature distribution in TEHL line contacts. But only considered the line contact, the point contact is not considered.

Recently, an inverse model has been widely applied in many design and manufacturing problems in which some of the surface conditions cannot be measured. It can also be used to indirectly obtain desired parameters without spending a lot of experimental funds. The parameters can approach to the true value. However, this method used in the inverse TEHL of point contact problems are lacking in the literature. Hence, in this paper, the inverse approach is extended to calculate the mean oil film temperature, surface temperature distributions, and pressure-viscosity index in TEHL of point contact problems using inverse method.

THEORETICAL ANALYSIS

2.1 Reynolds equation

As shown in Fig. 1, the contact geometry of two balls can be reduced to the contact geometry as a ball and a flat surface. For the steady state, thermal EHL point contact problems, the Reynolds equation can be expressed in the following dimensionless form as:

$$\frac{\partial}{\partial X}\left(\frac{\bar{\rho}H^3}{\bar{\eta}}\frac{\partial P}{\partial X}\right)+\frac{\partial}{\partial Y}\left(\frac{\bar{\rho}H^3}{\bar{\eta}}\frac{\partial P}{\partial Y}\right)=\lambda\frac{\partial}{\partial X}(\bar{\rho}H) \tag{1}$$

Where

$$\lambda=\frac{12\eta_0\bar{u}R_x^2}{b^3 p_h}$$

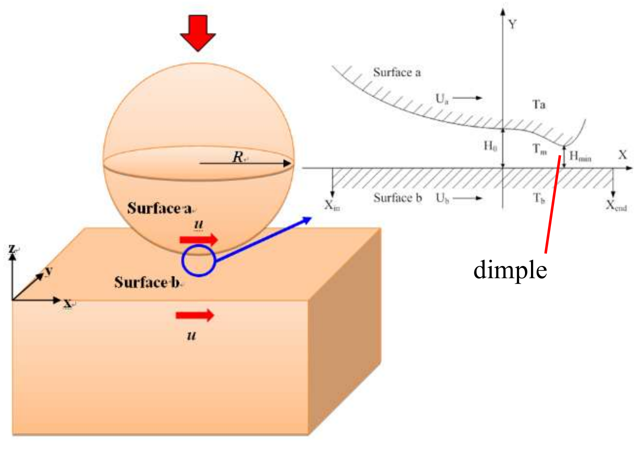

Fig. 1 The geometry of an EHL point contact

2.2 Rheology equation

In rheology equations, the mass density and the viscosity of lubricants related to pressure and temperature can be expressed as (Dowson and Higginson, 1966, Roelands et al., 1963):

$$\bar{\rho}=\frac{\rho}{\rho_0}=1+\frac{0.6\times10^{-9}p}{1+1.7\times10^{-9}p}\left[1-\beta(T_m-T_0)\right] \tag{2}$$

$$\overline{\eta} = \exp\{(9.67 + \ln\eta_0)[-1 + (1 + 5.1\times10^{-9} p)^{z^*}] - \gamma(T_m - T_0)\} \quad (3)$$

where z is the pressure-viscosity index, β is thermal expansivity of lubricant, γ is temperature-viscosity coefficient of lubricant.

2.3 Direct inverse method for calculating pressure

It has been known that the film thickness in a TEHL contact is the sum of the elastic deformation of the surfaces and the gap distance between two rigid surfaces. In the TEHL point contact, the film thickness in the dimensionless form is given as:

$$H_{i,j} = H_{00} + \frac{(X_{i,j}^2 + Y_{i,j}^2)}{2} + \frac{2}{\pi^2}\sum_{k=1}^{n_x}\sum_{l=1}^{n_y} K_{ikjl} P_{kl} \quad (4)$$

Discretizing the domain with equi-distant mesh size Δ, Eq. (4) can be approximated by

$$H_{i,j} - \frac{(X_{i,j}^2 + Y_{i,j}^2)}{2} - H_{00} = \frac{2}{\pi^2}\sum_{k=1}^{n_x}\sum_{l=1}^{m_y} K_{ijkl} P_{kl} \quad (5)$$

In this equation, the coefficients K_{ikjl} can be determined by assuming the uniform pressure over the various areas in the contact area. For half of the domain, K_{ikjl} can be expressed as:

$$K_{ikjl} = \quad (6)$$

$$\left|X_P\right|\ln\left(\frac{Y_p+\sqrt{X_p^2+Y_p^2}}{Y_m+\sqrt{X_p^2+Y_m^2}}\right)+\left|Y_m\right|\ln\left(\frac{X_m+\sqrt{Y_m^2+X_m^2}}{X_P+\sqrt{Y_m^2+X_p^2}}\right)$$

$$\left|X_m\right|\ln\left(\frac{Y_m+\sqrt{X_m^2+Y_m^2}}{Y_p+\sqrt{X_m^2+Y_p^2}}\right)+\left|Y_p\right|\ln\left(\frac{X_p+\sqrt{Y_p^2+X_p^2}}{X_m+\sqrt{Y_p^2+X_m^2}}\right)+$$

$$\beta\left\{\left|X_P\right|\ln\left(\frac{\overline{Y}_p+\sqrt{X_p^2+\overline{Y}_p^2}}{\overline{Y}_m+\sqrt{X_p^2+\overline{Y}_m^2}}\right)+\left|\overline{Y}_m\right|\ln\left(\frac{X_m+\sqrt{\overline{Y}_m^2+X_m^2}}{X_P+\sqrt{\overline{Y}_m^2+X_p^2}}\right)+\right.$$

$$\left.\left|X_m\right|\ln\left(\frac{\overline{Y}_m+\sqrt{X_m^2+\overline{Y}_m^2}}{\overline{Y}_p+\sqrt{X_m^2+\overline{Y}_p^2}}\right)+\left|\overline{Y}_p\right|\ln\left(\frac{X_p+\sqrt{\overline{Y}_p^2+X_p^2}}{X_m+\sqrt{\overline{Y}_p^2+X_m^2}}\right)\right\}$$

where

$$X_p = X_i - X_k + \frac{\Delta}{2}, \quad X_m = X_i - X_k - \frac{\Delta}{2}$$

$$Y_p = Y_j - Y_l + \frac{\Delta}{2}, \quad Y_m = Y_j - Y_l - \frac{\Delta}{2}$$

$$\overline{Y}_p = Y_j + Y_l + \frac{\Delta}{2}, \quad \overline{Y}_m = Y_j + Y_l - \frac{\Delta}{2}$$

$\beta = 0, for\ k = 1$(along the x-axis).

$\beta = 1,$ the others.

The normal load on the ball is assumed to be constant, thus the constant H_{00} can be obtained from the dimensionless force balance equation as:

$$\int_{-\infty}^{\infty}\int_{-\infty}^{\infty} P(X,Y)dXdY = \frac{2\pi}{3} \quad (7)$$

or in the discretized form as:

$$\frac{2\pi}{3} = \Delta^2\sum_{k=1}^{n_x}\sum_{l=1}^{n_y}\gamma P_{kl} \quad (8)$$

Where $\gamma = 1$, for $k = 1$ (along the x-axis),

$\gamma = 2$, the others.

Once the film shape is measured, the pressure distribution can be calculated from Eqs (5) and (8) or in a matrix form as:

$$\mathbf{H} = \mathbf{DP} \quad (9)$$

or

$$\begin{bmatrix} H_{i,j} - \dfrac{X_{i,j}^2 + Y_{i,j}^2}{2} \\ 2\pi/3\Delta^2 \end{bmatrix} = \begin{bmatrix} \dfrac{2}{\pi^2}K_{ijkl} & 1 \\ \gamma & 0 \end{bmatrix}\begin{bmatrix} P_{kl} \\ H_{00} \end{bmatrix} \quad (10)$$

This system equation includes $(n_x)\times(n_y)+1$ equations and unknowns. The matrix **D** is a full square matrix. In this paper, if the pressure distribution is calculated from Eq. (9), then it is called the direct inverse method.

2.4 Inverse approach for calculating pressure

In order to avoid the small fluctuation in calculating the pressure, the pressure distribution can be assumed to be a polynomial function. Moreover, since the pressure distribution is symmetric with respect to the x-axis, it can be expressed as:

$$P_{kl} = \sum_{n=0}^{l_x}\sum_{m=0}^{l_y} a_{nm}(X_k - c_3)^n (Y_l - c_4)^{2m} \quad (11)$$

where a_{nm} is an undetermined coefficient, l_x and l_y are positive integers, and c_3 and c_4 are constants. For the cases studied in this paper, c_3 and c_4 are set to zero. By using this polynomial function, Eq. (9) becomes

$$\mathbf{H} = \mathbf{DFA} \quad (12)$$

or

$$\begin{bmatrix} H_{i,j} - \dfrac{X_{i,j}^2 + Y_{i,j}^2}{2} \\ 2\pi/3\Delta^2 \end{bmatrix} = \begin{bmatrix} \dfrac{2}{\pi^2}K_{ijkl} & 1 \\ \gamma & 0 \end{bmatrix}\begin{bmatrix} P_{kl} \\ H_{00} \end{bmatrix}\begin{bmatrix} f_{k\ln m} & 0 \\ 0 & 1 \end{bmatrix}\begin{bmatrix} a_{nm} \\ H_{00} \end{bmatrix}$$

(13)

The **D** can be constructed from the elastic deformation theory, and **H** can be got by measurement equipment. Hence, if n measured points are employed, then **H** is $n+1$ column matrix, and **D** is a $(n+1)\times(k+1)$ matrix, where $k = n_x \times n_y$. It is obvious that **F** is a $(k+1)\times(l+1)$ matrix, and **A** is a $(l+1)$ column matrix, where $l = (l_x+1)\times(l_y+1)$ Generally, l_x is less than 9, and l_y is less than 5 in the present study.

If the unknown variables a_{nm} and H_{00} are given, the estimated film thickness can be calculated from Eq. (12). It is obvious that the estimated film thickness is different from the measured one. Hence, to obtain the smallest error between the measured and estimated film thickness, the linear least-squares method is employed here. The least-squares criterion requires the following function to be minimized.

$$g = (\mathbf{H}^{\text{estimated}} - \mathbf{H}^{\text{measured}})^{\mathrm{T}} (\mathbf{H}^{\text{estimated}} - \mathbf{H}^{\text{measured}}) \quad (14)$$

The best value for **A** can be determined from

$$\frac{\partial g}{\partial \mathbf{A}} = 0 \quad (15)$$

Then, the governing equation for the best value of **A** can be obtained as

$$\mathbf{A} = \left[(\mathbf{DF})^{\mathrm{T}} (\mathbf{DF}) \right]^{-1} (\mathbf{DF})^{\mathrm{T}} \mathbf{H} \quad (16)$$

In this equation, $(\mathbf{DF})^{T}(\mathbf{DF})$ is a $(l+1)\times(l+1)$ matrix. As a result, it can save much computation time in calculating **A** because l is less than 50 in the present study. The variables a_{nm} can be obtained from Eq. (16), the pressure distribution can be calculated from Eq. (11). Furthermore, since the pressure has been expressed as the polynomial form, the small fluctuation in the pressure can be eliminated.

2.5 Temperature calculation

The temperature distribution within an oil film can be solved by the energy equation subject to appropriate boundary conditions. Neglecting heat convection across the film and circumferential conduction in the film, the energy equation for point contact problems may be written as:

$$\frac{\partial}{\partial z}(\kappa \frac{\partial T}{\partial z}) = \rho c_p (u \frac{\partial T}{\partial x} + v \frac{\partial T}{\partial y}) - T\beta (u \frac{\partial p}{\partial x} + v \frac{\partial p}{\partial y}) - \eta [(\frac{\partial u}{\partial z})^2 + (\frac{\partial v}{\partial z})^2] \quad (17)$$

By integrating the momentum equation across the film thickness and substituting the boundary conditions z=0, $u = u_b, v = 0$, z=h, $u = u_a, v = 0$ the velocity equation can be calculated. Adding the velocity equations to Eq. (17) and integrating the resultant energy equation across the film thickness using the boundary conditions z=0, $t = t_b$, z=h, $t = t_a$, the mean oil film temperature can be expressed as:

$$t_m = \frac{t_a + t_b}{2} + (\rho c_p \frac{\partial t_m}{\partial x} - \beta t_m \frac{\partial p}{\partial x})[\frac{h^4}{120k\eta}(\frac{\partial p}{\partial x}) - \frac{u_a + u_b}{24k} h^2] + (\rho c_p \frac{\partial t_m}{\partial y} - \beta t_m \frac{\partial p}{\partial y})[\frac{h^4}{120\eta k}(\frac{\partial p}{\partial y})] + \frac{h^4}{240\eta k}[(\frac{\partial p}{\partial x})^2 + (\frac{\partial p}{\partial y})^2] + \frac{\eta (u_a - u_b)^2}{48k} \quad (18)$$

or in dimensionless form as:

$$\overline{T}_m = \frac{(\overline{T}_a + \overline{T}_b)}{2} + C_1 \overline{\eta} + C_2 \frac{\overline{\rho} H^4}{\overline{\eta}} (\frac{\partial P}{\partial X}\frac{\partial \Psi_1}{\partial X} + \frac{\partial P}{\partial Y}\frac{\partial \Psi_1}{\partial Y}) + (C_3 - C_4 \Psi_1)\frac{H^4}{\overline{\eta}}[(\frac{\partial P}{\partial X})^2 + (\frac{\partial P}{\partial Y})^2] - C_5 \overline{\rho} H^2 (C_7 \frac{\partial \Psi_2}{\partial X} + \frac{\partial \Psi_3}{\partial X}) + C_6 H^2 \frac{\partial P}{\partial X}(C_7 \Psi_2 + \Psi_3) \quad (19)$$

where

$$t_m = \frac{1}{h}\int_0^h t\, dz \quad (20)$$

$$\overline{T} = \frac{T}{T_0} - 1 \quad (21)$$

$$\Psi_1 = 1.2\overline{T}_m - 0.1(\overline{T}_a + \overline{T}_b) + 1 \quad (22)$$

$$\Psi_2 = \overline{T}_m + \frac{1}{6}(\overline{T}_a - \overline{T}_b) + 1 \quad (23)$$

$$\Psi_3 = \overline{T}_m + \frac{1}{6}(\overline{T}_b - \overline{T}_a) + 1 \quad (24)$$

$$C_1 = \frac{\eta_0 (u_a - u_b)^2}{12kT_0}, C_2 = \frac{\rho_0 c_p p_h b^6}{144\eta_0 k R_x^4},$$

$$C_3 = \frac{p_h b^6}{144\eta_0 k R_x^4 T_0}, C_4 = \frac{\beta p_h^2 b^6}{144\eta_0 k R_x^4},$$

$$C_5 = \frac{\rho_0 c_p b^3}{24kR_x^2}, C_6 = \frac{\beta p_h b^3}{24kR_x^2}, \quad C_7 = \frac{u_a}{u_b}$$

The energy equation requires the surface temperatures of the balls as its boundary conditions. The problem of the surface temperature of a semi-infinite solid subjected to a moving heat source was first solved by Carslaw and Jaeger (1959). Therefore, the boundary conditions for Eq. (19) can be expressed as:

$$\overline{T}_b(X,Y) = \overline{T}_{b0} + \frac{\kappa\sqrt{b}}{T_0\sqrt{\pi\rho_b c_b k_b u_b}} \frac{T_0 R}{b^2} \int_{X_{in}}^{X} \left.\frac{\partial \overline{T}}{\partial Z}\right|_{Z=0} \frac{dX'}{\sqrt{X - X'}} \quad (25)$$

$$\overline{T}_a(X,Y) = \overline{T}_{a0} + \frac{\kappa\sqrt{b}}{T_0\sqrt{\pi\rho_a c_a k_a u_a}} \frac{T_0 R}{b^2} \int_{X_{in}}^{X} -\left.\frac{\partial \overline{T}}{\partial Z}\right|_{Z=1} \frac{dX'}{\sqrt{X - X'}} \quad (26)$$

$$\overline{T}_m = \overline{T}_0, \text{ at } X = -\infty \quad (27)$$

Once the film shape is measured, the pressure distribution can be calculated from Eq. (9) using direct inverse method. In addition, the variables a_m can be calculated from Eq. (16). The pressure distribution can be calculated from Eq. (11), and the estimated film thickness can be calculated from equation (12) using present inverse approach.

Under the condition that the properties of lubricant and balls are given, since the mass density and the viscosity of lubricants are the functions of the pressure and mean temperature, so the initial mean temperature must be guessed. The Newton-Raphson method and the Gauss-Seidel iteration are employed to calculate the mean temperature distribution and the surface temperature distributions of the balls from Eqs. (2), (3), (9), and (19)-(27), or (2), (3), (11), (12), (16), and (19)-(27).

2.6 Inverse approach for calculating pressure-viscosity index

In order to increase the algorithm stability, the least-squares method must be employed here to calculate the optimum value of the pressure-viscosity index in the computational domain. The least-squares criterion requires the following function to be minimized. The Reynolds Eq. (1) and the Energy Eq. (19) can be rewritten as

$$\theta = \sum_{i=1}^{n_x} \sum_{j=1}^{m_y} \{ [\psi_{1ij}\overline{\eta}_{ij} + \psi_{2ij}\overline{\eta}_{ij}^2 - \frac{\partial \overline{\eta}_{ij}}{\partial P_{ij}}]^2 + [C_{1ij}\overline{\eta}_{ij} + \frac{\zeta_{1ij}}{\overline{\eta}_{ij}} + \zeta_{2ij}]^2 \} \tag{28}$$

where

$$\psi_1 = \frac{\overline{\rho}H^3(\frac{\partial^2 P}{\partial X^2} + \frac{\partial^2 P}{\partial Y^2}) + \frac{\partial(\overline{\rho}H^3)}{\partial X}\frac{\partial P}{\partial X} + \frac{\partial(\overline{\rho}H^3)}{\partial Y}\frac{\partial P}{\partial Y}}{\overline{\rho}H^3\left[\left(\frac{\partial P}{\partial X}\right)^2 + \left(\frac{\partial P}{\partial Y}\right)^2\right]} \tag{29}$$

$$\psi_2 = \frac{-\lambda\frac{\partial(\overline{\rho}H)}{\partial X}}{\overline{\rho}H^3\left[\left(\frac{\partial P}{\partial X}\right)^2 + \left(\frac{\partial P}{\partial Y}\right)^2\right]} \tag{30}$$

$$\zeta_1 = C_2\overline{\rho}H^4(\frac{\partial P}{\partial X}\frac{\partial \Psi_1}{\partial X} + \frac{\partial P}{\partial Y}\frac{\partial \Psi_1}{\partial Y}) + H^4(C_3 - C_4\Psi_1)[(\frac{\partial P}{\partial X})^2 + (\frac{\partial P}{\partial Y})^2] \tag{31}$$

$$\zeta_2 = -C_5\overline{\rho}H^2(C_7\frac{\partial \Psi_2}{\partial X} + \frac{\partial \Psi_3}{\partial X}) + C_6H^2\frac{\partial P}{\partial X}(C_7\Psi_2 + \Psi_3) + \frac{(\overline{T}_a + \overline{T}_b)}{2} - \overline{T}_m \tag{32}$$

The functions ψ_1, ψ_2, ζ_1 and ζ_2 can be calculated at each grid point by using the finite difference method for all derivatives. Hence, substituting Eq. (3) into Eq. (28), the optimum value for z' can be determined from

$$\frac{\partial \theta}{\partial z'} = 0 \tag{33}$$

The Gauss-Seidel and over-relaxation technique are employed in solving the system equations. Since the pressure has been expressed as the polynomial form, the fluctuation in the pressure can be eliminated. Furthermore, the fluctuation in the measured film thickness and temperature also can be eliminated. Consequently, the pressure-viscosity index becomes very stable. After the new z is obtained, the apparent viscosity can be calculated from equation (3). Furthermore, the pressure-viscosity index must be updated by iteration method to calculate accurate temperature distribution and apparent viscosity until convergence. The flow chart for the present inverse approach is shown in Fig.2.

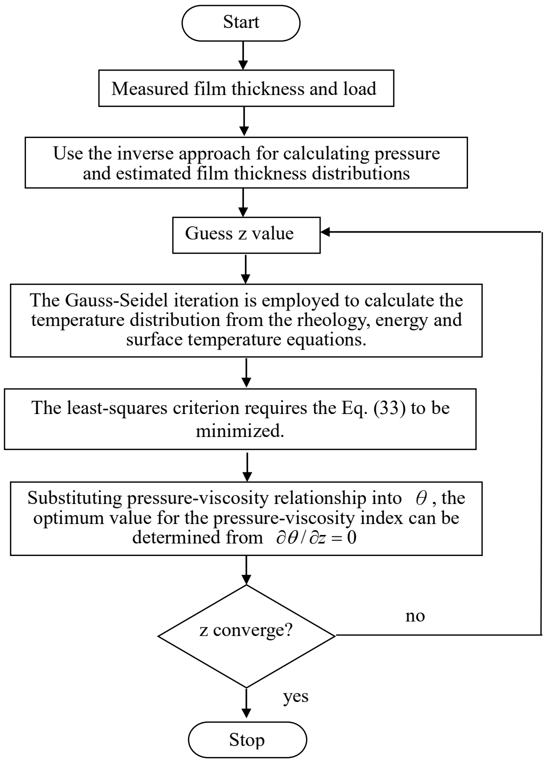

Fig. 2 Flow diagram of the present inverse approach

RESULTS AND DISCUSSION

3.1 Direct inverse method

In this study, the solutions of the film thickness and the pressure in the lubricated contacts are solved numerically by Lee et al. [14] using the lubricants and balls properties given in Tables 1 and 2. Which are referred to the 'exact' solution. Typical problem with $W = 1.93\times10^{-7}, U = 8.64\times10^{-12}$, and G = 3500 is solved. A grid size of 33×97 grid in the half domain is used to evaluate the pressure and temperature rise distributions within the lubricated contact region. Contour plot of the film thickness and measured points are shown in Fig. 3. In solving the thermal EHL point-contact problems, the coupled Reynolds equation, energy equation, load balance equation, film thickness equation, rheology equations and surface temperature equations must be solved simultaneously.

Table 1 Properties of lubricant

G (Material parameter)	3500.0
Inlet temperature of lubricant, K	313.0
Inlet viscosity of lubricant, *Pa-s*	0.04
Inlet density of lubricant, kg/m^3	846.0
Pressure viscosity coefficient, 1/GPa	15.91
Temperature-viscosity coefficient, 1/K	6.4E-4
Thermal conductivity of lubricant, W/m-K	0.14
Specific heat of lubricant, J/Kg-K	2000.0
Pressure-viscosity coefficient (Roelands)	0.4836

J. CSME Vol.47, No.4 (2026)
10.29979/JCSME.202608_47(4).0003

Table 2 Properties of balls

Equivalent radius, m	0.02
Thermal conductivity of rollers, W/m-K	47.0
Specific heat of rollers, J/Kg-K	460.0
Density of rollers, kg/m^3	7850.0
Elastic modulus of rollers, GPa	200
Poisson's ratio of rollers	0.3

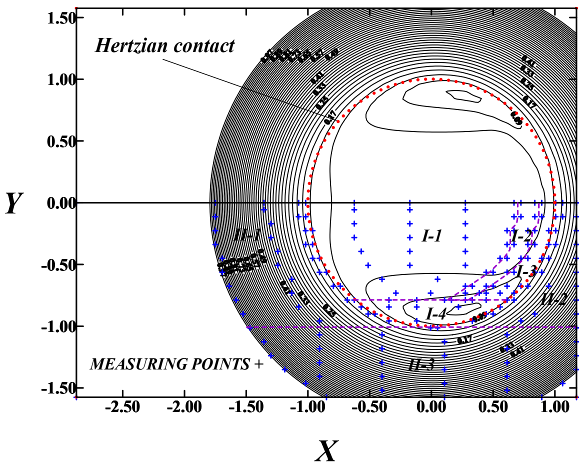

Fig.3 Film thickness map, and regions and measuring points on the computational domain. (+++ Measuring points, ● ● ● Hertzian circle)

When the measured points are the same as the estimated points, it is not necessary to use the series form to represent the pressure distribution. Hence, the solution obtained from Eqs. (2), (3), (9) and (19)-(27) are called the solution of the direct inverse method. By using the direct inverse method, Figs. 4 and 5 show the pressure distribution along the X-axis at different Y position, and along the Y-axis at different X position using 833 uniform measured points in the half domain, respectively.

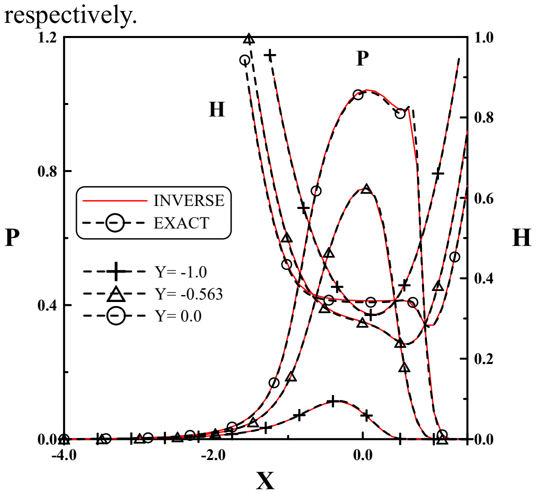

Fig. 4 Pressure and film thickness distributions along the X-axis using direct inverse method.

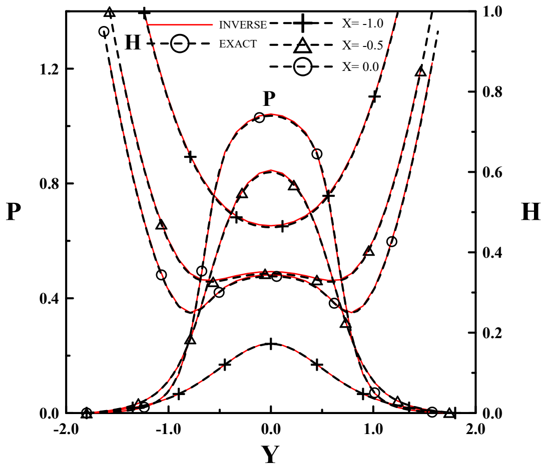

Fig. 5 Pressure and film thickness distributions along the Y-axis using direct inverse method.

Figs. 6 and 7 show the temperature rise distribution along the X-axis at different Y position, and along the Y-axis at different X position using 833 uniform measured points in the half domain, respectively.

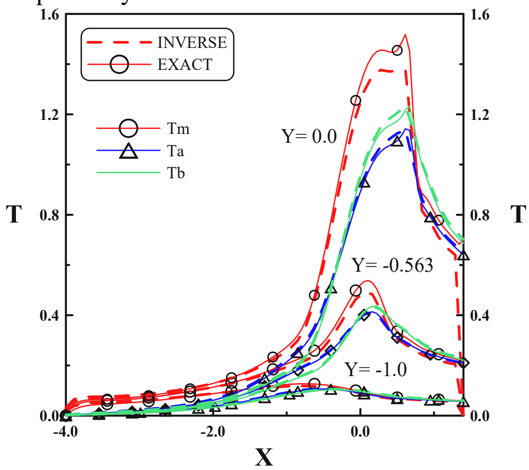

Fig. 6 Temperature distributions along the X-axis using direct inverse method.

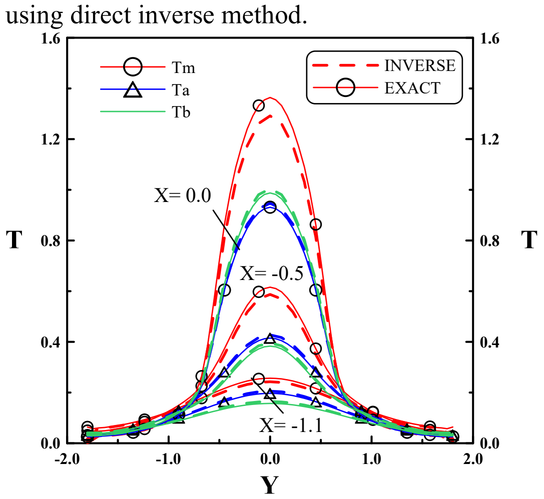

Fig. 7 Temperature rise distributions along the Y-axis using direct inverse method.

Figs. 8 and 9 show the pressure distribution along the X-axis at different Y position, and along the Y-axis at different X position using 3201 uniform measured points in the half domain, respectively. Figs. 10 and 11 show the temperature rise distribution along the X-axis at different Y position, and along the Y-axis at different X position using 3201 uniform measured points in the half domain, respectively.

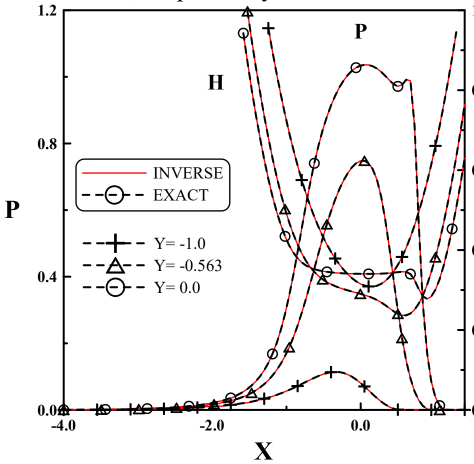

Fig. 8 Pressure and film thickness distributions along the X-axis using direct inverse method.

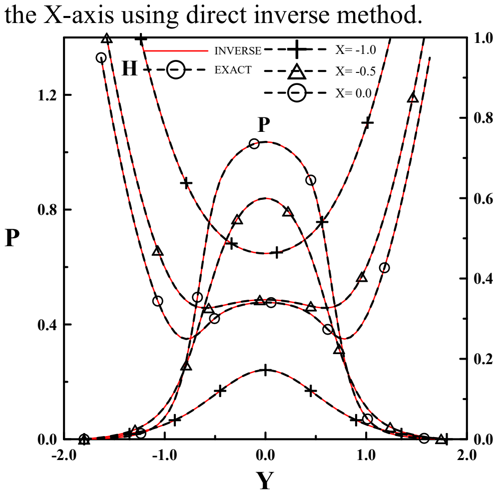

Fig. 9 Pressure and film thickness distributions along the Y-axis using direct inverse method.

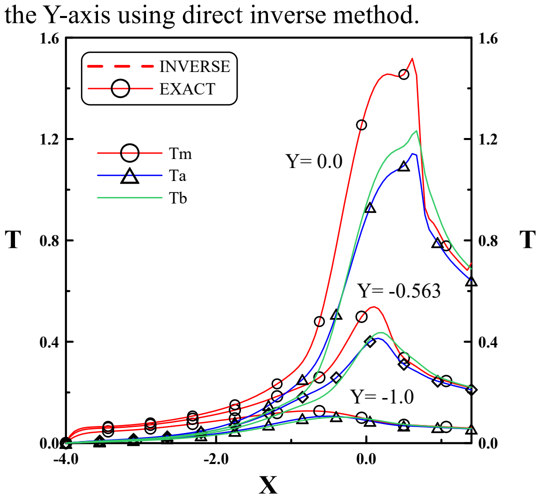

Fig. 10 Temperature distributions along the X-axis using direct inverse method.

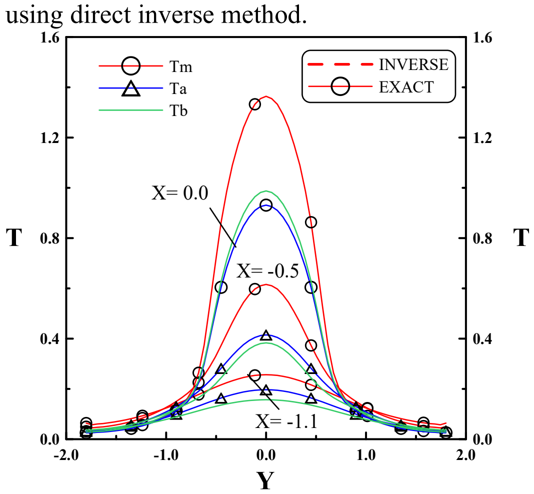

Fig. 11 Temperature distributions along the Y-axis using direct inverse method.

In these figures, the input data is the film thickness at different measured points. It is obvious that with increasing the number of measured points, the solution approaches the 'exact' numerical solution. When the 833 uniform measured points are used, results show that the estimated pressure and temperature rise values have some errors especially in the center and the pressure spike regions, the temperature error values are greater than the pressure error values. When the measured points (3201) are increased, results show that the estimated pressure and temperature rise values become quite good in the center and the pressure spike regions. It is clear that the direct inverse method requires a lot of measured points.

Usually, the measurement error always occurs in the measurement process. This measurement error makes the estimation away from the 'exact' numerical solution. In this study, the measured film thickness is generated from the pre-selected 'exact' numerical film thickness with the measurement error, and it can be expressed as:

$$H_i^{measured} = H_i^{exact} + \sigma H_c \lambda_i \tag{34}$$

where λ_i is a random number, H_c is the dimensionless central film thickness, and σ is the dimensionless standard deviation of the measurement error.

Figs. 12 and 13 show the effect of the measurement error (σ =0.01) on the dimensionless pressure distribution along the X-axis at different Y position, and along the Y-axis at different X position using 3201 uniform measured points in the half domain, respectively. Fig. 14 shows the dimensionless pressure profile obtained using the direct inverse approach with the measurement error (σ =0.01). It is seen from this figure that the pressure fluctuations can be found everywhere.

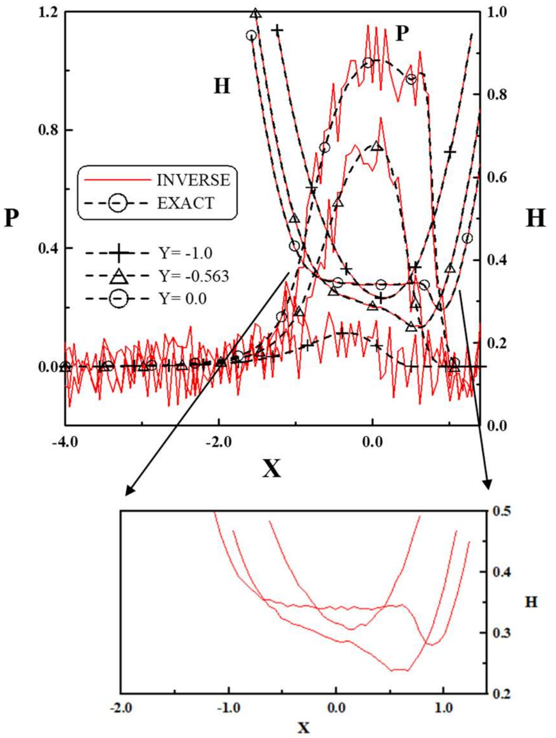

Fig. 12 Pressure and film thickness distributions with measurement error (σ =0.01) along the X-axis using direct inverse method.

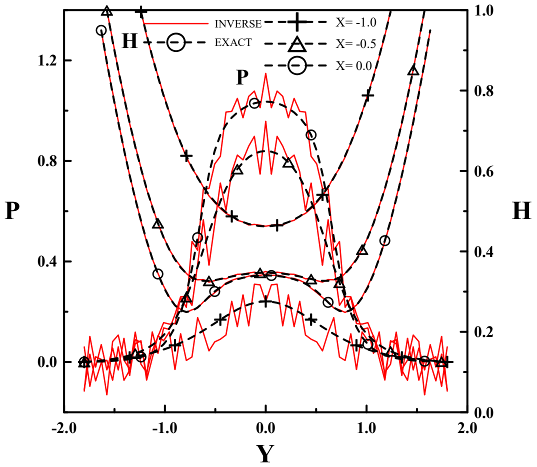

Fig. 13 Pressure and film thickness distributions with measurement error (σ =0.01) along the Y-axis using direct inverse method.

It is seen from these figures that the measurement error (σ =0.01) on the oil film significantly influences the pressure distribution, and the perturbation of film measurement error (σ =0.01) can result in a local pressure change. As a result, the pressure fluctuations can be found everywhere. If these pressure distributions and measured oil film distributions are used to solve the temperature rise distributions, the errors in the temperature rise should be greater. The iterative process can easily diverge. Therefore, the allowable measurement error in oil film must be very small using direct inverse method.

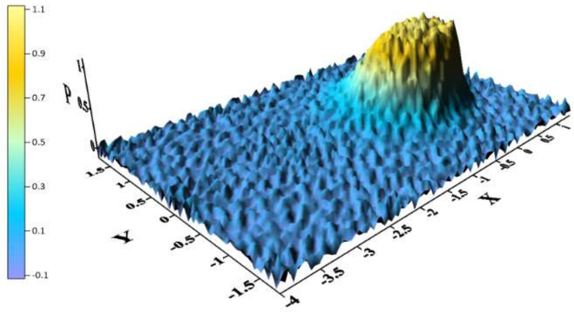

Fig.14 Pressure distribution with measurement error (σ =0.01) by using direct inverse method.

3.2 Inverse approach solution for pressure and temperature rise distributions

To overcome the above problems, the oil film error causes the pressure error, which makes the temperature calculation easy to diverge. Hence, this paper proposes an inverse approach. It is known that a pressure spike appears in the dimple region of the film shape in the viscous EHL problems. Hence, the inverse approach is proposed to obtain an accurate pressure and temperature rise distributions, it is necessary to divide the domain into a few regions due to the singular point at the pressure spike. In this paper, the domain is divided into two regions including the Hertz contact area and outside the Hertz contact area. The Hertz contact area is divided into three regions including central region, dimple region, and horseshoe shaped region. The outside Hertz contact area is divided into three regions including inlet region, outlet region, and side outlet region, as shown in Fig. 3. Different regions have different polynomials that can be incorporated into the system calculation.

The unknown pressure distribution is approximated by a polynomial form shown in Eq. (11) with c = -3, a_0 = 0. The measured points in the film thickness are shown in Fig. 3. By using Eq. (16), the polynomial coefficients can be calculated. Substituting these coefficients into Eq. (11), the estimated pressure distribution can be calculated. The measurement error on the oil film significantly influences the pressure and temperature rise distributions. Therefore, the estimated film shape can be calculated from the calculated pressure using Eq. (12). As mentioned above, the mean temperature distribution and the surface temperature distributions of the balls can be calculated from Eqs. (2), (3), (11), (12), (16), and (19)-(27).

It was discussed in Figs. 12-14 that the measurement error in the film thickness (σ =0.01) can result in pressure and temperature rise fluctuations everywhere. To obtain a smooth curve in the pressure and temperature rise distributions, the inverse approach is employed to solve this case. Figs. 15-20 present typical results obtained using the inverse approach when all the operating parameters are the same as those used in Figs. 12-14. In these figures, the domain for the estimated pressure is divided into seven regions using 171 measured points in the film thickness. To obtain more accurate pressure and temperature rise distributions, it is necessary to increase the number of measured points in the dimple region and in the pressure spike region, as shown in Fig. 3.

Figs. 15 and 16 show that the inverse approach can obtains a reasonably smooth curve for the pressure distributions along the X-axis at different Y position, and along the Y-axis at different X position using 171 measured points in the half domain, respectively. Figs. 17 and 18 show that the inverse approach obtains a reasonably smooth curve for the temperature rise distributions along the X-axis at different Y position, and along the Y-axis at different X position using 171 measured points in the half domain, respectively. It can be seen from these figures that the pressure and temperature rise fluctuations can be Eliminated. The oil film measurement error can also be corrected.

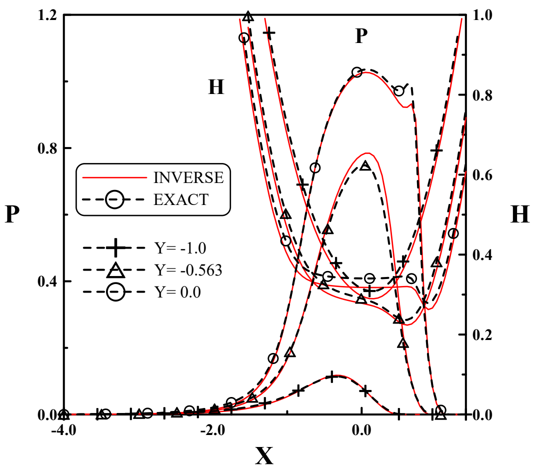

Fig. 15 Pressure and film thickness distributions with measurement error (σ =0.01) along the X-axis using inverse approach.

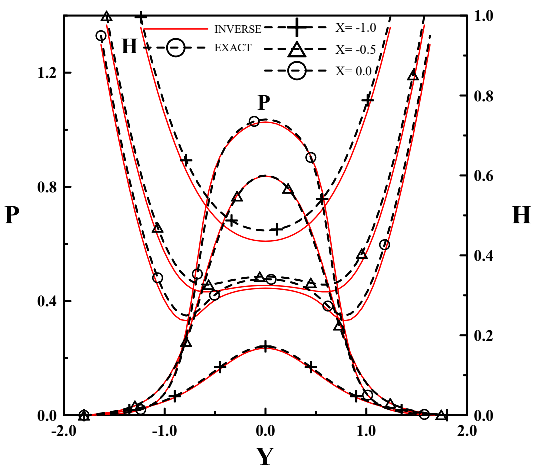

Fig. 16 Pressure and film thickness distributions with measurement error (σ =0.01) along the Y-axis using inverse approach.

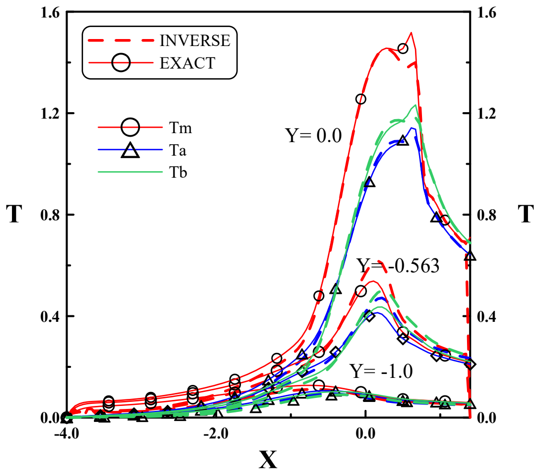

Fig. 17 Temperature distributions with measurement error (σ =0.01) along the X-axis using inverse approach.

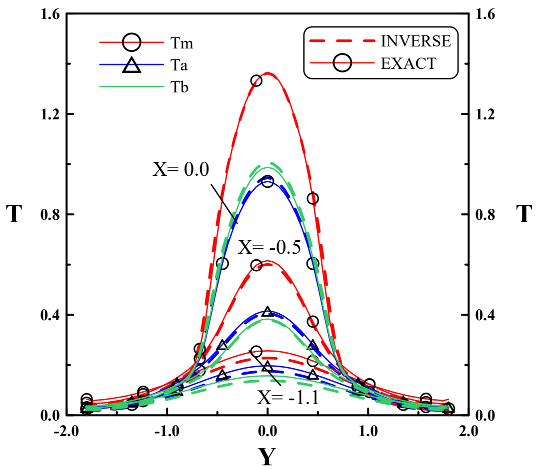

Fig. 18 Temperature distributions with measurement error (σ =0.01) along the Y-axis using inverse approach.

Figs. 19 and 20 show the dimensionless pressure profile obtained using the inverse approach with the measurement error (σ =0.01) using 171 measured points in the half domain, respectively. It is seen from this figure that the pressure and temperature distributions are smooth.

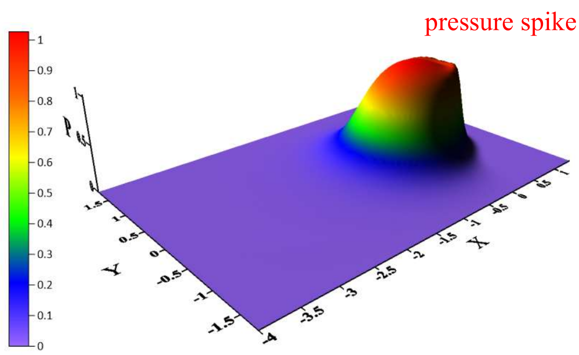

Fig.19 Pressure distribution with measurement error

(σ =0.01) by using inverse approach.

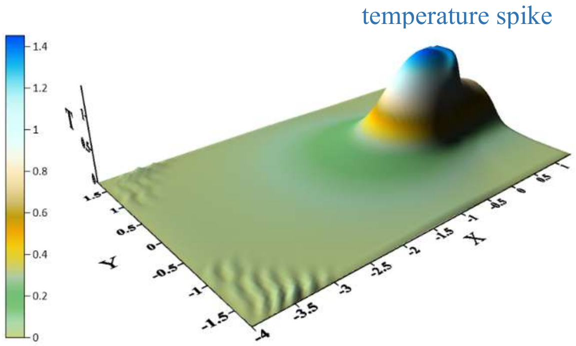

Fig.20 Temperature distribution with measurement error (σ =0.01) by using inverse approach.

3.3 Inverse solution for apparent viscosity

As mentioned above, since the mass density and the viscosity of lubricants are the functions of the pressure and mean temperature, so the mean temperature of lubricant must be known. In addition, the pressure-viscosity index, the thermal expansivity and the temperature-viscosity coefficient of lubricant are unknown. If they are unknown simultaneously, the algorithm is complex and unstable. Therefore, in this paper, the thermal expansivity and the temperature-viscosity coefficient of lubricant must be given, so the pressure-viscosity index must be guessed initially in order to calculate temperature distribution.

The oil film measurement error will significantly influence the pressure distribution using direct inverse method. If the pressure distribution and oil film distribution are used to solve the temperature rise distribution, the errors in the temperature rise should be greater. The iterative process can easily diverge. The calculation of the pressure-viscosity index will also easily diverge. Therefore, this paper used present inverse method to solve the pressure distribution, the estimated film thickness distribution, and the temperature rise distribution shown in Figs. 8-11. They are used to solve Eq. (33) in seven regions. The relative error value of the pressure-viscosity index is 5.8%.

CONCLUSIONS

This paper proposed an inverse approach to estimate the pressure distribution, the temperature rise distribution, and the pressure-viscosity index in an TEHL point contact for the given film thickness. To obtain an accurate pressure, it is necessary to divide the domain into a few regions due to the singularity at the pressure spike. This approach overcomes the problems of pressure and temperature rise fluctuations and generates accurate results of pressure and temperature rise distribution from a small number of measured film thickness points, which also saves computing time. The simulation results show that the direct inverse method requires many measured points to obtain the correct pressure and temperature distribution, but the inverse approach can obtain accurate results with only a few measured points. For the film thickness measurement error, this approach also presents a smooth curve of the pressure and temperature distributions with a small error in the inlet, pressure spike, and outlet regions. Without the measurement error in the film thickness, this approach provides quite good solution for the pressure-viscosity index. With the measurement error in the film thickness, this approach still gives a quite good solution for the pressure-viscosity index, but the direct method provides much larger error for the temperature distribution and the pressure-viscosity index. This present inverse approach can tolerate larger the film thickness measurement error.

The current pressure measurement technology cannot reach the sub-millimeter level and cannot measure detailed pressure distribution, but can measure the average pressure value between contact bodies. The contact area in the sub-millimeter range. With the advancement of technology, the pressure measurement accuracy can reach sub-millimeter in the future. The experimental values of pressure distribution can be compared with the present value of pressure distribution. Furthermore, the experimental value of temperature distribution can be compared with the present value of temperature distribution.

ACKNOWLEDGMENT

The authors would like to express their appreciation to the National Science and Technology Council (NSTC-113-2221-E-143-002) in Taiwan, R. O. C. for financial support.

REFERENCES

Astrom H. and Venner C. H., Soap thickener induced local pressure fluctuations in a grease lubricated elastohydrodynamic point contact, Proc. Instn. Mech. Engrs., Part J: J. of Eng. Tribology, 1994, 208, 191-198.

Ausherman V.K., Nagaraj H.S., Sanborn D.M., Winer W. O., Infrared temperature mapping in elastohydrodynamic lubrication. Trans. ASME J. Lubr. Technol., 1976, 98(2), 236–242.

Carslaw H. S. and Jaeger J. C., Conduction of Heat in Solids, Oxford University Press, 1959.

Chu L.M., Hsu H.C., Lin J.R., Chang Y.P., Inverse Approach for Calculating Temperature in EHL of Line Contacts, Tribology International, 2009, 42, 1154-1162.

Cyriac F., Lugt P.M., Bosman R., Padberg C.J., Venner C.H., Effect of Thickener Particle Geometry and Concentration on the Grease EHL Film Thickness at Medium Speeds, Tribology

Letters, 2016;61:18.
Dowson D. and Higginson G.R., Elastohydrodynamic Lubrication, Pergamon Press, 1966, 88-92.
J.O., Larsson R., Venner C.H., Determination of viscosity and pressure in an elastohydrodynamic rolling contact by using optical interferometry: a theoretical study, Proc. Instn. Mech. Engrs., Part J: J. of Eng. Tribology, 1996, 210, 259-268.
Kannel J.W., Zugaro F.F., and Dow T.A., A method for measuring surface temperature between rolling/sliding steel cylinders. Trans. ASME J. Lubr. Technol., 1978, 100(1), 110–114.
Lee R.T., Chu H.M., Chiou Y.C., Inverse approach for estimating pressure and viscosity in the elastohydrodynamic lubrication of circular contacts, Proc. Instn Mech. Engrs, Part J: J. of Eng. Tribology, 2003, 217, 1-12.
Lu J, Reddyhoff T, Dini D, 3D Measurements of Lubricant and Surface Temperatures Within an Elastohydrodynamic Contact, Tribol Lett, 2018;66:7.
Marx N, Guegan J, Spikes H.A., Elastohydrodynamic film thickness of soft EHL contacts using optical interferometry, Tribology International, 2016, 99, 267-277.
Paul G.R. and Cameron A., A high-pressure microviscometer based on refractive index, Proc. R. Soc., Ser. A, 1972, 331, 171-184.
Roelands C. J. A., Vlugter J. C. and Watermann H. I., The viscosity temperature pressure relationship of lubricating oils and its correlation with chemical constitution, ASME Journal of Basic Engineering, 1963, 601-606.
Safa M.M.A, Anderson J.C, Leather J.A., Transducers for pressure, temperature and oil film thickness measurement in bearings. Sens. Actuators, 1982–83, 3, 119–128.
Turchina V., Sanborn D.M., Winer W.O., Temperature measurements in sliding elastohydrodynamic point contacts. Trans. ASME J. Lubr. Technol., 1974, 96(3), 464–469.
Wong P.L., Lingard S., Cameron A., The high pressure impact microviscometer, STLE Tribology Trans., 1992, 35(3), 500-508.
Yagi K., Kyogoku K., Nakahara T., Experimental investigation of effects of slip ratio on elastohydrodynamic lubrication film related to temperature distribution in oil films, Proc. Instn. Mech. Engrs., Part J: J. of Eng. Tribology, 2006, 220(4) 353-363.
Yagi K., Kyogoku K., Nakahara T., Relationship Between Temperature Distribution in EHL Film and Dimple Formation, ASME Trans J Tribology, 2005, 127(3) 658-665.

NOMENCLATURE

b	semiwidth of hertzian contact (m)
C_p	ecific heat of the lubricant (J kg^{-1} K^{-1})
C_a, C_b	specific heat of rollers a and b (J kg^{-1} K^{-1})
E'	equivalent elastic modulus (Pa)
G	dimensionless material parameter, $\alpha E'$
h	film thickness (m)
H	dimensionless film thickness, hRx/b^2
Hc	dimensionless central film thickness
H_{00}	dimensionless constant defined in Eq. (4)
K_{ijkl}	discretized kernel in Eq. (5)
k	thermal conductivity of lubricant (W m^{-1} K^{-1})
k_a, k_b	thermal conductivity of rollers a, b (W m^{-1} K^{-1})
p	pressure (Pa)
p_h	maximum hertzian pressure (Pa)
P	dimensionless pressure, p/p_h
R_x	reduced radius of curvature in x-direction (m)
T	temperature (K)
T_m	mean temperature of lubricant film (K)
T_a, T_b	surface temperature of rollers a and b
$\overline{T}$	dimensionless temperature, T/T_o
u_a, u_b	surface velocity of rollers a and b (m s^{-1})
$\overline{u}$	average rolling velocity (m s^{-1})
U	dimensionless speed parameter, $\eta_0\overline{u}/E'R_x$
w	load (N)
W	dimensionless load, $W = w/E'R_x^2$
x,y	coordinate (m)
X,Y	dimensionless coordinate, $X=x/b$, $Y=y/h$,
z'	Roelands' pressure-viscosity index
Δ	distance between two neighboring grid points
η	viscosity of lubricant (Pa-s)
η_0	viscosity of lubricant at ambient pressure (Pa-s)
$\overline{\eta}$	dimensionless viscosity, η/η_0
λ	dimensionless viscosity parameter, $\lambda = 12\eta_0\overline{u}R_x^2/b^3p_h$
λ_i	random number
ρ	density of lubricant (kg m-3)
ρ_0	inlet density of lubricant (kg m-3)
ρ_a, ρ_b	density of rollers a and b (kg m-3)
$\overline{\rho}$	dimensionless density of lubricant, ρ/ρ_0
β	thermal expansivity of lubricant (K-1)
γ	temperature-viscosity coefficient of lubricant (K-1)
σ	dimensionless standard deviation of the measured error